Received: 7 October 2022 | Revised: 5 April 2023 | Accepted: 18 May 2023

DOI: 10.1002/jbm.b.35286

RESEARCH ARTICLE

Osteoblast and bacterial cell response on RGD peptide-functionalized chitosan coatings electrophoretically deposited from different suspensions on Ti13Nb13Zr alloy

Łukasz Pawłowski[1] | Szymon Mania[2] | Adrianna Banach-Kopeć[2] | Michał Bartmański[1] | Anna Ronowska[3] | Kacper Jurak[4] | Aleksandra Mielewczyk-Gryń[5] | Natalia Karska[6] | Sylwia Rodziewicz-Motowidło[6] | Andrzej Zieliński[1]

[1]Institute of Manufacturing and Materials Technology, Faculty of Mechanical Engineering and Ship Technology, Gdańsk University of Technology, Gdańsk, Poland

[2]Department of Chemistry, Technology, and Biotechnology of Food, Faculty of Chemistry, Gdańsk University of Technology, Gdańsk, Poland

[3]Department of Laboratory Medicine, Medical University of Gdańsk, Gdańsk, Poland

[4]Department of Electrochemistry, Corrosion and Materials Engineering, Faculty of Chemistry, Gdańsk University of Technology, Gdańsk, Poland

[5]Institute of Nanotechnology and Materials Engineering, Faculty of Applied Physics and Mathematics, Gdańsk University of Technology, Gdańsk, Poland

[6]Department of Biomedical Chemistry, Faculty of Chemistry, University of Gdańsk, Gdańsk, Poland

Correspondence
Łukasz Pawłowski, Institute of Manufacturing and Materials Technology, Faculty of Mechanical Engineering and Ship Technology, Gdańsk University of Technology, Narutowicza 11/12, 80-233 Gdańsk, Poland.
Email: lukasz.pawlowski@pg.edu.pl

Abstract

Metallic materials for long-term load-bearing implants still do not provide high antimicrobial activity while maintaining strong compatibility with bone cells. This study aimed to modify the surface of Ti13Nb13Zr alloy by electrophoretic deposition of a chitosan coating with a covalently attached Arg-Gly-Asp (RGD) peptide. The suspensions for coating deposition were prepared in two different ways either using hydroxyacetic acid or a carbon dioxide saturation process. The coatings were deposited using a voltage of 10 V for 1 min. The prepared coatings were examined using SEM, EDS, FTIR, and XPS techniques. In addition, the wettability of these surfaces, corrosion resistance, adhesion of the coatings to the metallic substrate, and their antimicrobial activity (*E. coli*, *S. aureus*) and cytocompatibility properties using the MTT and LDH assays were studied. The coatings produced tightly covered the metallic substrate. Spectroscopic studies confirmed that the peptide did not detach from the chitosan chain during electrophoretic deposition. All tested samples showed high corrosion resistance (corrosion current density measured in nA/cm^2). The deposited coatings contributed to a significant increase in the antimicrobial activity of the samples against Gram-positive and Gram-negative bacteria (reduction in bacterial counts from 99% to, for CS-RGD-Acid and the *S. aureus* strain, total killing capacity). MTT and LDH results showed high compatibility with bone cells of the modified surfaces compared to the bare substrate (survival rates above 75% under indirect contact conditions and above 100% under direct contact conditions). However, the adhesion of the coatings was considered weak.

KEYWORDS
antibacterial properties, bioactivity, chitosan, electrophoretic deposition, RGD peptide, titanium alloy

1 | INTRODUCTION

Research efforts are still underway to modify materials for bone implants. They are currently focused mainly on modifying their surface to provide their high osteointegration properties while maintaining strong antimicrobial activity.[1,2] Among the modified materials, titanium and its alloys are leading the way. Ti13Nb13Zr alloy, due to its chemical composition (lack of Al and V that can cause bone softening and damage to the nervous system) and suitable mechanical properties similar to human bone, is one of the preferred candidates for the design of long-term load-bearing implants.[3]

The surface of Ti13Nb13Zr alloy is subject to modification by mechanical treatment (grinding, sandblasting, polishing), chemical treatment (etching), electrochemical treatment (oxidation), or covered with coatings using methods such as electrophoretic deposition (EPD), dip coating, spin coating, sol–gel, or gas-phase deposition.[4–7] For implants, the electrophoretic method is increasingly used, allowing irregularly shaped materials to be easily coated. Unfortunately, the layers and coatings produced in this way do not meet all the requirements for implants. Usually, the deposited coatings show poor adhesion to the metallic substrate, which results in their rapid failure at the stage of implant insertion into the human body.[8] The composition of the coatings is also a problem, and it is often difficult to obtain a surface with high osteointegration and a strong antibacterial effect.[9]

Chitosan (CS) being a natural biopolymer is widely used in pharmaceutical, food, and implant applications. There are several references in the literature regarding the fabrication of CS coatings on metallic surfaces using the EPD method with an analysis of the effect of the process parameters used on the coating properties.[10,11] CS is often subjected to additional modifications by mixing with other biopolymers, and functionalization with nanoparticles or peptides. The surfaces of biomaterials are modified with peptides to improve their biocompatibility and better integration with surrounding tissues by promoting the adhesion and survival of selected cell types.[12–14]

The most widely studied cell adhesion-promoting peptide for applications in the biomaterials field is a three-amino acid arginine-glycine-aspartic acid (Arg-Gly-Asp) sequence termed RGD. RGD has proved to be highly effective in promoting the attachment of numerous cell types to various materials. RGD is the primary binding domain for integrins present in extracellular matrix (ECM) proteins such as fibronectin, vitronectin, and fibrinogen.[15] The RGD sequence can bind to many integrin species. It appears that αVβ3, αVβ5, and αIIβ3 are the integrins most reported to be involved in the bone function and RGD sequence binding.[16] The activity of the RGD sequence exhibits mainly during the extracellular signal transduction and proliferation. It has been shown that the RGD peptide-functionalized biomaterials effectively support the bioactivity of materials used for bone regeneration.[17] The use of RGDs, compared to native ECM proteins, also minimizes the risk of immune reactivity. Another benefit is that the synthesis of RGD peptides is relatively simple and inexpensive, making it easier to implement in clinical practice. Finally, RGD peptides can be attached to the surfaces of materials at a controlled density.[18,19] Finally, RGD functionality is usually preserved during the processing and sterilization required in biomaterial synthesis, many of which cause protein denaturation.

The combination of CS with RGD peptide is increasingly reported. CS nanoparticles with RGD peptide were investigated as a pH-responsive targeted drug delivery carrier in cancer therapy.[20] RGD peptide was also coupled to poly(ethylene glycol)-modified CS micelles that were used for tumor-targeting treatment.[14] There have also been reported attempts to fabricate scaffolds from RGD-conjugated cross-linked CS for the differentiation of mesenchymal stem cells.[21] Studies of surface modification of titanium by covalently grafted CS with immobilized RGD peptide for better osteointegration and reduction of bacterial adhesion can also be found.[19] CS with RGD-based systems are often enriched with other biopolymers such as hyaluronic acid and deposited on titanium.[22] Data on the production of such coatings by the EPD method on titanium or titanium alloys are scarce. The literature mostly mentions suspensions of CS in organic and inorganic acids, but there are numerous reports that this type of liquid medium can result in reduced adhesion and proliferation of various cell populations to coatings produced in this manner.[23] Coatings prepared from such suspensions still contain acids after drying, hence they dissolve slowly in water. An interesting solution is preparing chitosan hydrogels by saturating the suspension of its microcrystalline sediment with gaseous CO_2. Formed carbonic acid is responsible for dissolving the chitosan and is easily released (in the form of H_2O and CO_2) during the drying of the coating.[24–26]

The purpose of the research presented in this paper was to modify the electrophoretic deposition on the titanium surface of the CS-based coatings with attached RGD peptide molecules. In particular, two different suspension preparation methods, using dissolved hydroxyacetic acid or a novel CO_2 saturation process, were applied. The physical–chemical and biological properties of the CS-RGD coatings such as their roughness and morphology, surface microstructure, chemical and phase composition, adhesion to the titanium substrate, corrosion resistance, and biocompatibility in vitro determined by the behavior of human osteoblast cells. The fabrication of such coatings with the EPD method implementing two different suspension preparation methods to deposit the coatings on the Ti13Nb13Zr alloy has never been studied and described in the literature. Especially, the authors have assumed that such coatings, together with other important features, will demonstrate bacteria-killing ability better than the other material solution based on chitosan and could significantly improve patient comfort and reduce the risk of postoperative bacterial infections.

2 | MATERIALS AND METHODS

2.1 | Preparation of samples

The round samples, 20 mm in diameter and 4 mm in height, were made of the Ti13Nb13Zr alloy (Bibus Metals, Dąbrowa, Poland), and its chemical composition is given in Table 1. Then they wet ground (Saphir 330, ATM GmbH, Mammelzen, Germany) using emery papers

TABLE 1 The chemical composition of a substrate material (given by the manufacturer)

Element	Nb	Zr	Fe	C	N	O	Ti
wt %	13.00	13.00	0.05	0.04	0.02	0.11	rest

(Struers Company, Cracow, Poland), No. 800 as the last. Finally, they were washed with isopropanol (99.9%, POCH S.A., Gliwice, Poland) and distilled water (HLP 5, Hydrolab, Straszyn, Poland).

2.2 | Synthesis of peptide

The peptide was obtained by the standard solid-phase synthesis (Liberty Blue, CEM Corporation, USA) on TentaGel R RAM resin (capacity of 0.67 mmol/g, Rapp Polymere GmbH, Germany) following the Fmoc-chemistry strategy. The synthetic peptide was purified using reversed-phase high-performance liquid chromatography (RP-HPLC) equipped with two Knauer K1001 pumps and a Gilson fraction collector with a UV–vis detector. The 10 mm × 250 mm Kromasil C-8 column (particle diameter: 5 μm, pore size: 30 nm) was applied for purification at linear gradients of an acetonitrile-water mixture (containing 0.1% [v/v] TFA) used as eluent and a flow rate of 5 mL/min. The presence of peptide was indicated at a wavelength of 223 nm. The purity of the obtained peptide was higher than 99% as estimated by RP-HPLC.

2.3 | Functionalization of chitosan with RGD peptide

In the first stage, the chitosan in form of a scaffold was covalently functionalized with a maleimidoglycine linker, in line with the procedure described in [patent application no. P.443979 and P.442878, Patent Office of the Republic of Poland]. After the removal of the unreacted substrates, the chitosan-maleimidoglycine scaffold underwent drying under a vacuum. Subsequently, RGD peptide terminated with additional N-terminal cysteine amino acid was deposited, by click chemistry reaction between -SH group of cysteine and maleimidoglicyne moiety, on chitosan scaffold in the peptide solution stirred for 24 h at room temperature. CS-RGD was filtered with gooch G3 and dried under vacuum for 1 h. The degree of chitosan deposition by the RGD peptide was 10%.

2.4 | Preparation of suspensions

The suspensions for the deposition of CS-RGD coatings were prepared by two different preparation methods. The CS-RGD powder was either dissolved directly in hydroxyacetic acid (Avantor Performance Materials S. A., Gliwice, Poland) or additionally subjected to a CO_2 saturation process. In detail, using the first approach, 0.1 g of CS-RGD powder was dissolved in 100 mL of 1% hydroxyacetic acid. The concentration of the biopolymer and acid was chosen based on previous works,[8,13,27] which ensured that homogeneous coatings were obtained, tightly covering the metallic substrate. In the second method, such solution was treated with 0.5 M sodium hydroxide solution (Avantor Performance Materials S. A., Gliwice, Poland) until the pH equal to 8 was reached and CS-RGD powder precipitated. The obtained CS-RGD sediment was separated from a liquid using a glass filter set equipped with a vacuum pump (ROCKER 600, Alfachem Sp.z o.o., Lublin, Poland). Then the sediment was washed twice with distilled water (5:1 m/m concerning the weight of the sediment). After filtration, the precipitate was weighed and put into distilled water to achieve 0.1 wt. pct. of polymer concentration, then subjected to a CO_2 saturation process at mechanical mixing of liquid using a hollow shaft agitator (BIO-MIXBMX-10, Gdańsk, Poland). Both solutions were finally mechanically mixed with the same stirrer until the chitosan was completely dissolved. These two transparent solutions were used to deposit the CS-RGD coatings. According to the method of preparation of the suspensions, the samples were designated as CS-RGD-Acid (hydroxyacetic acid) and CS-RGD-CO_2 (CO_2 saturation process).

2.5 | Electrophoretic deposition of CS-RGD coatings

The coatings were fabricated for both approaches in the same condition by electrophoretic deposition performed in a two-electrode system. The Ti13Nb13Zr alloy sample constituted the cathode, while a mesh platinum electrode was an anode, keeping a distance between them 10 mm. A direct current source (MCP Corp., Shanghai, China) was used to make EPD. Based on our earlier research on EPD-made CS-based coatings,[27,28] the EPD was performed at a voltage of 10 V for 1 min. Low values of voltage and deposition time, as confirmed by previous studies,[27,28] resulted in a reduction of the water electrolysis phenomenon and intensive formation of hydrogen bubbles on the cathode, which significantly reduces the uniformity of the deposited coatings. After deposition, samples were washed only with distilled water and dried in ambient air for at least 24 h.

2.6 | Coatings characterization

The surface morphology was examined by scanning electron microscopy (SEM, FEI Quanta FEG 250, Hillsboro, OR, USA). Before SEM imaging, the coated samples were sputtered with a thin 10 nm thick gold layer using a DC magnetron sputtering system (EM SCD 500, Leica, Vienna, Austria) in a pure Ar plasma condition.

The elemental composition was carried out with an energy-dispersive X-ray spectroscopy (EDS, Edax Inc, Mahwah, NJ, USA).

The X-ray photoelectron spectroscopy (XPS) study was executed with an Escalab 250Xi (ThermoFisher Scientific, USA) calibrated for adventitious C1s (284.6 eV) employing an Al Kα anode. The resulting

data were processed using Avantage software supplied by the manufacturer.

The surface roughness was measured on a 50 × 50 μm area using an atomic force microscope (AFM, NaniteAFM, Nanosurf AG, Liestal, Switzerland). The values of the Sa parameter (arithmetic mean deviation) were determined based on the 3D roughness distribution maps as the means of three values.

The surface wettability was assessed with a goniometer (Attention Theta Life, Biolin Scientific, Espoo, Finland) using the falling drop method and distilled water of 2 μL in volume. The measurements of contact angle were made after 10 s from drop fall. OneAttension software was applied for the calculation of contact angles.

The thicknesses of the coatings were counted with a thickness meter (SN100146594, Helmut Fischer GmbH, Germany) and expressed as means of 5 measurements for each investigated sample.

The adhesion of coatings was ascertained by a scratch test (NanoTest™Vantage device, Micro Materials, Wrexham, UK). The scratches were each time 500 μm long. The applied force stepwise increased from 0 to 120 mN at a rate of 1.3 mN/s. The appearance of complete delamination of the coating from the substrate surface was established by analyzing the friction force - normal force relationship and then a critical force (Lc) was found for each scratch.

The corrosion resistance was determined by a potentiodynamic method using a three-electrode system composed of the test sample of 1 cm^2 in area, a platinum counter electrode, a saturated calomel electrode SCE, and a potentiostat/galvanostat (Atlas 0531, Atlas Sollich, Gdańsk, Poland). The tests were made in a simulated body fluid (SBF, 37°C, the chemical composition by[29]). The open circuit potential (OCP) was determined after 1 h of exposure to the corrosive solution. Afterward, the voltage–current corrosion curves were established in the potential range of −1.0 ÷ 1.0 V, at a potential change rate of 1 mV/s, and making measurements at first in the cathodic and then in the anodic direction. By Tafel extrapolation, the values of corrosion potential (E_{corr}) and corrosion current density (j_{corr}) were found.

The ASTM E2149 test with a slight modification, previously described in,[30] was used to evaluate the antimicrobial activity of the tested samples. The activity of the samples was verified against *Escherichia coli* K-12 PCM 2560 (NCTC 10538) and *Staphylococcus aureus* PCM 2054 (American Type Culture Collection - ATCC 25923) from the Polish Collection of Microorganisms (Ludwik Hirszfeld Institute of Immunology and Experimental Therapy, Polish Academy of Sciences, Wrocław, Poland). The tested bacteria were subcultured at first. These bacterial cultures grew in a tryptic soy broth medium (Sigma-Aldrich, Saint Louis, MO, USA) and were subjected to incubation for 24 h at 37°C. The subsequent step involved obtaining the appropriate number of bacterial cells (1.5×10^7 to 5×10^7 CFU/mL). Utilizing a spectrophotometer (at a wavelength of 600 nm), dilutions of the bacterial culture suspension in phosphate-buffered saline (PBS) were made for obtaining an optical density of 0.08 ÷ 0.1. The examination area of the samples was 9.42 cm^2. Before testing, the surfaces of the samples were sterilized under UV light for 30 minutes on each side. Afterward, 0.18 mL of a previously prepared inoculum of the test strain was poured onto each sample together with polyethylene (PE) film, which acted as a negative control. Inoculated samples were covered with PE film to provide proper contact between the bacterial suspension and the tested material, followed by incubation for 24 h at 37°C. Following incubation, samples were placed in 10 mL of PBS solution and vortexed for 5 × 5 seconds. Cultures were performed by pour plate method with tryptic soy agar (TSA) medium upon making 10-fold dilutions in peptone water ($10^0 \div 10^8$). The plates were incubated for 24 h at 37°C. The number of cells was counted at the end of the incubation and varied from 0 ÷ 300 units. The number of cells in 1 mL was calculated according to the formula:

$$V_c = N \times D,$$

where V_c is the bacteria concentration, in colony-forming units per mL (CFU/mL), N is the average value from Petri dishes (CFU), and D is the dilution factor from the plates counted. Antimicrobial activity was calculated according to the equation:

$$R = \log B/C,$$

where B is the average of the number of viable cells on the control sample (CFU/mL), and C - is the average of the number of viable cells on the tested sample (CFU/mL). A percentage reduction of bacteria on a logarithmic scale (R) equal to 1, 2, and 3 means a reduction of 90%, 99%, and 99.9%, respectively.

For the cell culture test, the cellular model was human osteoblasts: hFOB 1.19 (RRID: CVCL 3708), obtained from ATCC. Cells were grown cultured in a 1:1 mixture of Ham's F12 medium and Dulbecco's Modified Eagle's Medium (without phenol red), supplemented with 1 mmol/L L-glutamine, 0.3 mg/mL G418, and 10% fetal bovine serum. The cells used for the experiments were from 5 to 8 passages. The cells were passed two times before each experiment. The cells were incubated at 34°C in a humidified atmosphere with 5% CO_2, and 95% air. To measure the direct effect of the titanium alloy surface modification the cells were directly seeded on the surface of each sample at a density of 0.15 mLn. Following, the cells were cultured for 24 at standard conditions. After the dedicated time, the viability tests were conducted. To measure the indirect effect of tested compounds, the cells were treated with the medium preconditioned with tested samples and incubated under identical conditions to the cell culture. The cells were seeded at a density of 0.012 mLn per well of a 96-well plate and were cultured at the standard conditions for 24 h. Following the medium was exchanged for an extract of the test material. The culture continued for the next 24 h.

The viability of the cells treated with the tested compounds was assayed by the MTT reduction test (3-[4,5-dimethylthiazol-2-yl]-2,5-diphenyltetrazolium bromide). This test measures the activity of mitochondrial enzymes, mainly succinate dehydrogenase. The 0.06 mmo/L of the MTT was added to the living cells that remained attached to the tested surface. The cells were incubated for the next 4 h to metabolize the dye. Finally, the blue product of the reaction was measured spectrophotometrically at 570 nm. The control cells were the ones attached to the not modified sample.

The mortality of the cells was assayed by the fractional NAD^+oxidoreductase (lactate dehydrogenase, LDH, EC 1.1.1.27) release test. LDH is the cytoplasmic enzyme that is released by the dead cells. Therefore after 24 h of the growth of the cells on the samples, the medium from the culture was collected where the activity of LDH was measured. The oxidation of NADH was spectrophotometrically determined at 340 nm.

2.7 | Statistical analysis

Statistical analysis of collected data was worked out by OriginPro software (8.5.0 SR1, OriginLab Corporation). The Shapiro–Wilk test was applied to prove a normal distribution of data. All results are expressed as mean ± standard deviation (SD). Statistical analysis was made out by one-way ANOVA, considering the Bonferroni correction, with a statistical significance of $p < .05$.

3 | RESULTS AND DISCUSSION

SEM images of the prepared samples are shown in Figure 1A. Examination of the bare substrate revealed a typical microstructure after grinding. In the case of coated samples, no significant differences were observed in the degree of surface coverage and smoothness of the coatings, despite the usage of different EPD suspension preparation methods. Slight transparency in the coating deposited from the hydroxyacetic acid suspension was visible, which may indicate that a thinner coating was obtained. Due

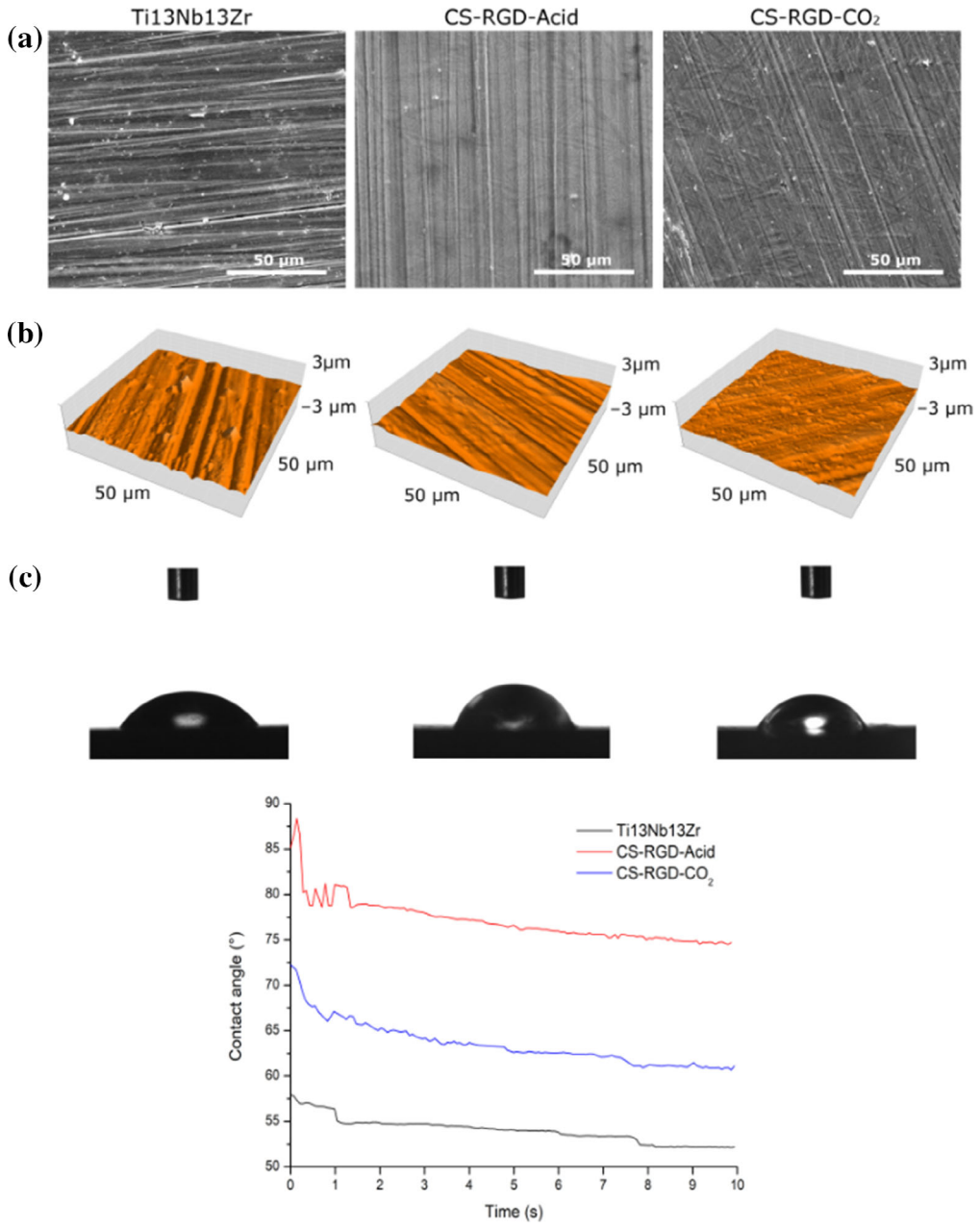

FIGURE 1 (A) SEM images of the surfaces, (B) surface roughness, and (C) wettability test results obtained for investigated samples.

to the use of lower EPD process parameters, i.e. voltage and deposition time, the electrolysis of water and formation of hydrogen bubbles on the cathode was limited, which translated into smoother surfaces. The results obtained confirmed previous observations.[11]

The obtained SEM images coincided with 3D roughness maps of the tested surfaces obtained by atomic force microscopy (Figure 1B). There was no significant difference in the value of the Sa parameter measured (Table 2) for the Ti13Nb13Zr substrate compared to the coated samples. In addition, these differences between samples were also not significant. So, the EPD suspension preparation method did not notably affect the surface roughness of the coatings.

Wettability test results (Figure 1C and Table 2) showed that all samples tested were hydrophilic. For all samples tested, the measured value of the contact angle decreased over time. Samples with coatings showed a significantly higher contact angle value compared to the titanium alloy substrate. There was also a significant difference in wettability between samples with coatings. The differences in the surface roughness of the coated samples were not remarkable, so the disparities in the wettability of these surfaces were most likely caused by the adoption of various methods for preparing EPD suspensions.

The chitosan hydrogels prepared for deposition differed in the pH value. The pH of the CO_2-saturated chitosan solution was about 6.5, while for chitosan dissolved in 1% hydroxyacetic acid it was lower by at least 2 units. The presence of hydroxyacetic acid increased the intensity of the water electrolysis process and the intensity of hydrogen secretion on the surface of the electrode, which hindered the polymer coating efficiency. Electrophoretic deposition of chitosan coatings was carried out using alcohol (methanol, ethanol, and isopropanol)-water mixtures with different contents of acetic acid by the Farrokhi-Rad team. They concluded that the EPD rate increased with acid content to the maximum and then decreased with its further addition. They also observed current density increase during EPD from solutions with higher acetic acid contents due to the enhanced water electrolysis.[31] The presence of residual acid in the CS-RGD-Acid sample can also be an explanation for the result of the contact angle measurement. Applying the drops to the material can cause partial dissolution of chitosan as a result of its protonation, and reduction of roughness. Unfortunately, this kind of observation is impossible to observe in non-dynamic measurements.

Coatings prepared by dissolving CS-RGD powder using CO_2 saturation showed greater thickness. Such an assumption was also supported by the results of SEM and AFM studies. The difference in the thickness of the deposited coatings may be due to the fact of increased aggregation of chitosan particles in hydroxyacetic acid suspension compared to the CO_2 saturation method. Literature data report that under similar deposition conditions, in the case of hydrochloric acid, for example, is much less effective in suppressing intermolecular aggregation compared to carbonic acid. This difference may be due to the higher intensity of fluctuations when chitosan is dissolved in CO_2. The large amount of dissolved CO_2 at high pressures provides strong local fluctuations of CS in suspension. As a result of the increased fluctuation intensity, the dispersion capacity of the fluid increases, resulting in a lower degree of aggregation of CS macromolecules.[24] During electrophoresis, the size and shape of the molecule affect the rate of migration in such a way - the larger the size, the slower rate at which the molecule will move through the suspension. In the case of the CS-RGD-CO_2 sample, CS particles were less agglomerated, and migrated faster toward the cathode, allowing more particles to reach the cathode in 1 min exposure, thus leading to a thicker coating compared to the CS-RGD-Acid sample.[32]

TABLE 2 Results of surface roughness, contact angle, and thickness measurements obtained for the tested samples; *significantly different from Ti13Nb13Zr sample; #significantly different from CS-RGD-Acid sample (ANOVA with Bonferroni correction $p < .05$)

Sample	Sa (nm)	Contact angle (°)	Coating thickness (μm)
Ti13Nb13Zr	108 ± 16	49.82 ± 5.74	-
CS-RGD-Acid	98 ± 14	72.01 ± 5.29*	0.42 ± 0.20
CS-RGD-CO_2	95 ± 9	65.18 ± 3.35*#	1.50 ± 0.07#

Figure 2A shows the infrared spectrum obtained for the coated samples. In both coatings, the individual maxima were quite clearly visible, however, the maxima relating to the peptide were weakly seen, as the degree of chitosan embedded with the peptide was low. However, the bands relating to chitosan would be observed. The band in the 3390–3360 cm^{-1} region corresponds to N-H and O-H stretching vibrations. Accordingly, the bands at about 2921 and 2877 cm^{-1} are responsible for symmetric and asymmetric C-H stretching. The presence of N-acetyl residues was confirmed by C=O stretching bands from amide I at about 1645 cm^{-1} and C-N stretching from amide III at 1325 cm^{-1}. The bands at about 1423 and 1375 cm^{-1}, respectively, refer to CH_2 bending and CH_3 symmetric deformations. The peak at 1153 cm^{-1} comes from the asymmetric stretching of the C-O-C bridge. The bands at 1066 and 1028 cm^{-1} are from C-O stretching.[33]

The spectra obtained for core levels C1s, O1s, and N1s measured for coated samples using the XPS technique are depicted in Figure 2B. Using curve-fitting analysis, the core level C1s spectrum was resolved into three components for both samples tested. Peak 1 for the binding energy of 285 eV referred to the aliphatic carbons (C-C) of the side chains of the RGD peptide. Peak 2 (286.4 eV) confirms the presence of O=C-C-N carbons of the peptide backbone, with the C-N carbons of the lysine groups. Peak 3 (288.1 eV), in turn, is due to the O=C-N carbons of the peptide and the O=C=O carbons of the aspartic acid group. The presence of the fourth peak at a binding energy of about 289.3 eV relating to bonds from aspartate and arginine noted in other references[34] was faintly apparent. Spectra for O1s for both samples revealed three peaks. The peaks for individual samples are slightly shifted concerning each other, possibly due to the method of preparing EPD suspensions. Peak 1 (530.5 eV) comes from oxygen from the oxide layer of the substrate material. Peak 2 (532.0 eV) comes from O=C oxygens of the peptide and the carboxylate group of aspartic acid and was more intense for the sample made from the hydroxyacetic acid suspension. Peak 3 potentially could be attributed to the

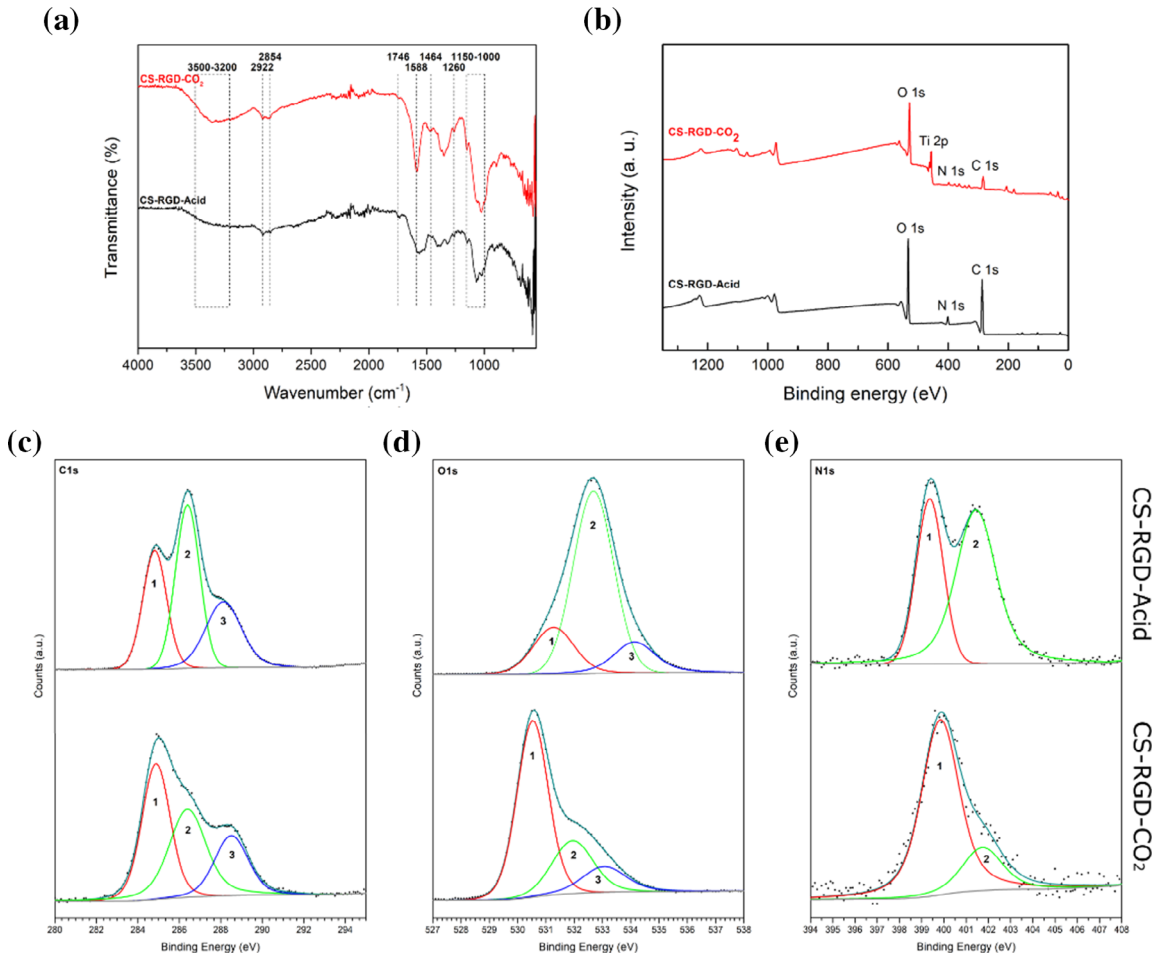

FIGURE 2 (A) FTIR spectra for samples with coatings, and (B) XPS survey obtained for CS-RGD-Acid and CS-RGD-CO_2 samples with (C) C1s, (D) O1s, and (E) N1s spectra (peaks described in the text).

oxygen of the C-O bonds. Two peaks were visible on the N1s spectra. Peak 1 (400.0 eV) was probably related to the C=N nitrogens of the arginine group. Peak 2 (402.0 eV), was due to the arginine groups. XPS examination confirmed that the peptide remained unseparated from the chitosan chain during the electrophoretic deposition of coatings.

Figure 3A and Table 3 collect the results to determine the adhesion of coatings to metallic substrates obtained from the scratch test. Based on the dependence of the friction force of the indenter in contact with the sample and the normal force at which the indenter penetrated the test surface, the value of the critical force (Lc) causing complete removal of the biopolymer coating from the titanium alloy substrate and the corresponding value of the friction force were determined. The determined values of the Lc force were relatively low indicating poor adhesion of both types of coatings. The weak adhesion of chitosan-based coatings has already been reported.[35] Attempts to mitigate this problem should become the subject of future research work. Possibly, an improvement in adhesion would be brought by additional roughening of the substrate surface before coating deposition, application of interlayer, or functionalization of the titanium alloy surface.[8] Adding another biopolymer and preparing the blend was also noted as a way to improve the adhesion of chitosan coatings.[36]

Corrosion study results are presented in Figure 3B (open circuit potential course and corrosion curves). The values of corrosion parameters obtained after the Tafel extrapolation procedure are collected in Table 3. All samples tested stabilized their potential after staying in the SBF solution for an hour. There were differences between the measured OCP values among the coated samples. A more positive value of −0.088 V was recorded for the CS-RGD-Acid sample in comparison to the CS-RGD-CO_2 sample (−0.329 V). The bare substrate with Ti13Nb13Zr achieved an intermediate OCP value equal to −0.176 V. The measured OCP values were close to the determined E_{corr} values. The CS-RGD-CO_2 sample showed the highest corrosion resistance with a j_{corr} value of 161 ± 49 nA/cm^2. It was a significantly lower value compared to the coated sample prepared from a suspension of CS in hydroxyacetic acid. In this case, the j_{corr} value was considerably higher even from a bare substrate. The CS-RGD-CO_2 coated sample, due to its greater thickness, most likely provided a better barrier separating the substrate material from the corrosive environment, which translated into higher corrosion resistance. For a much thinner CS-RGD-Acid coating, possibly the SBF solution in

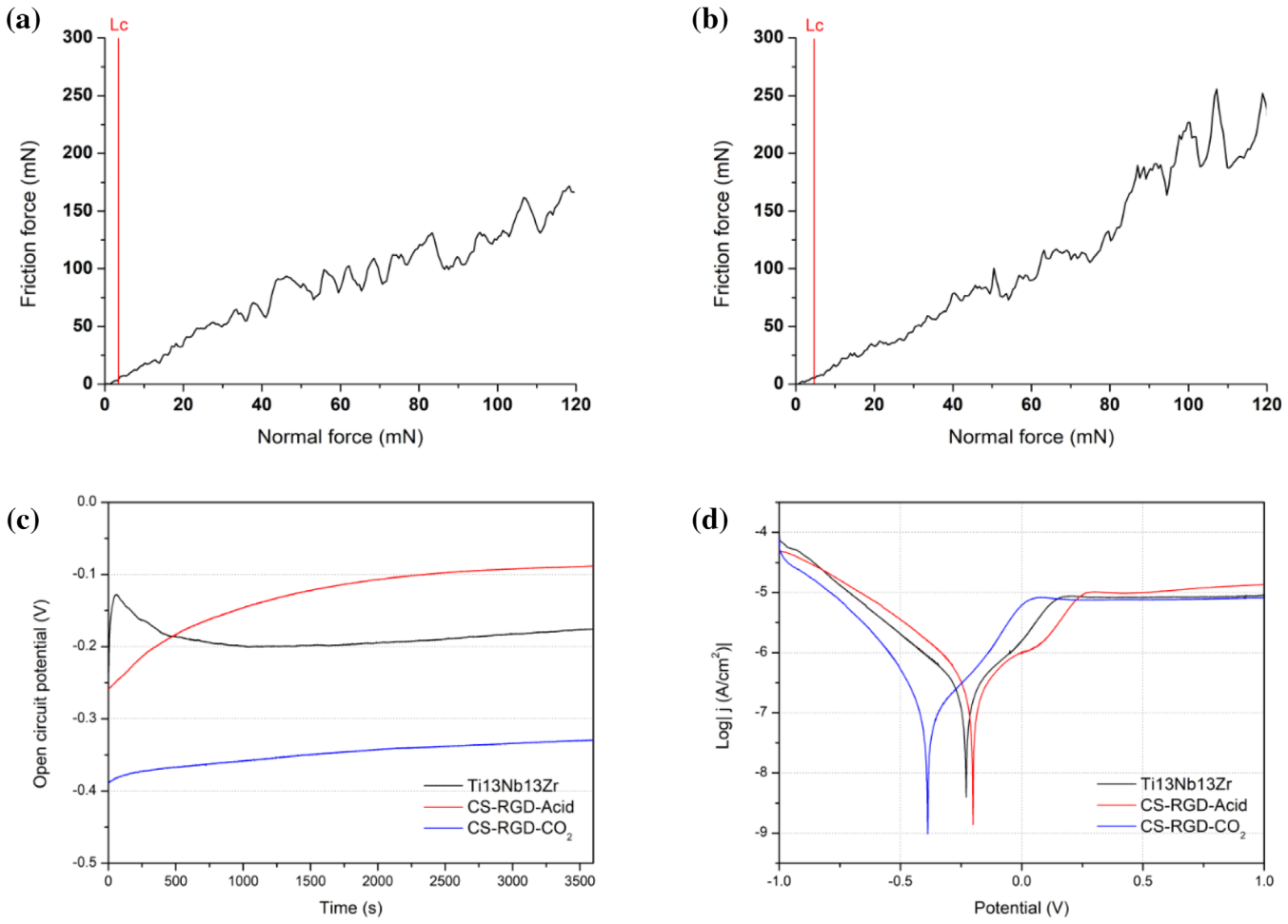

FIGURE 3 Curves of frictional force dependence as a function of normal force with the critical force (*Lc*) value marked, obtained during a single scratch of samples with (A) CS-RGD-Acid and (B) CS-RGD-CO_2 coatings, and the results of corrosion studies: (C) open circuit potential, and (D) corrosion curves.

	Scratch test results		Corrosion parameters	
Sample	Critical Force (mN)	Friction force (mN)	E_{corr} (V)	j_{corr} (nA/cm^2)
Ti13Nb13Zr	-	-	−0.227 ± 0.01	332 ± 48
CS-RGD-Acid	4.92 ± 1.01	7.42 ± 2.29	−0.201 ± 0.04*	654 ± 109*
CS-RGD-CO_2	5.19 ± 1.15	7.02 ± 2.13	−0.386 ± 0.02*#	161 ± 49*#

TABLE 3 Scratch test and corrosion study results obtained for prepared samples; *significantly different from Ti13Nb13Zr sample; #significantly different from CS-RGD-Acid sample (ANOVA with Bonferroni correction $p < .05$)

which the corrosion tests were conducted could penetrate the coating and intensify corrosion processes.

The results of investigating the antimicrobial activity of the produced coatings against *E. coli* and *S. aureus* are shown in Figure 4. Both proposed coatings showed high antimicrobial activity against Gram-positive and Gram-negative bacteria compared to the substrate subjected to grinding only. Stronger activity against the tested bacterial strains was noted for the sample with the CS-RGD coating deposited from suspension in hydroxyacetic acid. For the *S. aureus* bacteria, the reduction in the bacterial count was more than twice as high as the CS-RGD-CO_2 sample. Chitosan is probably primarily responsible for the antibacterial effect of the produced coatings. The mechanism of chitosan's antibacterial effect is not fully known, but most likely positively charged protonated amino groups of chitosan interact with the negatively charged cell wall of the bacteria and disrupt its continuity, resulting in leakage of intracellular components and its elimination. Hence, the importance of chitosan's molecular weight, degree of deacetylation, and coupling with other functional groups in maintaining its antimicrobial properties are crucial. There is evidence in the literature that the RGD peptide does not affect bacterial cells. No negative effects on the antimicrobial activity of systems containing the RGD peptide were observed.[19] Moreover, acid residues were likely present in coatings deposited from a suspension containing hydroxyacetic acid. An acidified environment can potentiate the antibacterial

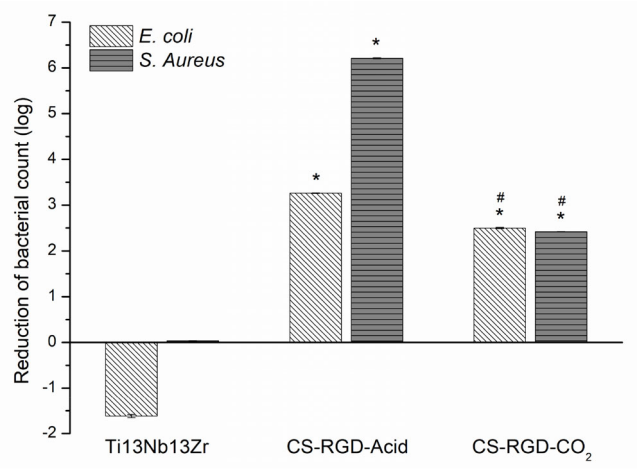

FIGURE 4 Antimicrobial activity results for a bare Ti13Nb13Zr substrate and samples with CS-RGD coatings; *significantly different from Ti13Nb13Zr sample; #significantly different from CS-RGD-Acid sample (ANOVA with Bonferroni correction $p < .05$).

effect,[37] hence a stronger antibacterial effect was observed in CS-RGD-Acid coatings. The difference in antibacterial effect against *E. coli* and *S. aureus* was probably due to the different cell wall structures of Gram-positive and Gram-negative cells.[30] Gram-negative bacteria contain a double cell membrane, compared to Gram-positive bacteria, which may have contributed to their greater survival rate when in contact with the test samples. Further studies are needed to accurately determine the antibacterial activity of the various coating components.

The use of highly biocompatible materials (such as chitosan) on a non-toxic titanium alloy substrate in the production of coatings should not cause a toxic cellular response. The studies conducted and the results of human osteoblast cell viability and LDH release shown in Figure 5 confirm the previous assumption. Cytotoxicity tests were performed under direct contact conditions (Figures 5B and D) and for different dilutions of the extract under indirect contact conditions (Figures 5A and C). The results of cell viability studies indicate high biocompatibility of the materials with survival rates above 75% under indirect contact conditions and above 100% under direct contact conditions. The critical limit is estimated to be 75%. Both for tests under direct and indirect conditions, this value was obtained. Tests indicate that the modification used does not affect cell viability under direct contact conditions. For indirect contact conditions, only for CS-RGD-Acid samples (dilution 1/1 and 1/5) and CS-RGD-CO_2 samples (dilution 1/1 and 1/2), a significant decrease in survival was observed. Still, the value is above 75%. The release of lactate dehydrogenase was below 30% for direct and indirect contact conditions. The study showed no differences between the modifications used. According to the statistical analysis, there were no significant differences between coated samples, but they were significantly different from the controls. The probable lower survival rate of hFOB 1.19 cells in contact with the CS-RGD-Acid coating (compared to the CS-RGD-CO_2 sample) could be due to the presence of the acetic acid residue used to prepare the EPD suspension in this coating.

Finally, it is important to decide which preparation procedure has given better results and what are advantages of both technologies over already proposed solutions are. Five such properties are worth considering: wettability, adhesion, corrosion resistance, antibacterial efficiency, and cytotoxicity.

Considering wettability, it is noticed that all coatings in this research have been hydrophilic. The differences between a substrate and two here investigated coatings can be neglected as they do not potentially affect the anticipated adhesion of cells. Such hydrophilicity is a necessary condition and has already been demonstrated at 35.6° for chitosan-gelatine hydrogel,[38] 60° for the catechol functionalized chitosan and gelatin with Ag nanoparticles,[39] for the silica xerogel/chitosan as varying from 7° to 34° with chitosan content and its fraction approaching 50%,[40] for silica-chitosan the contact angle changed from 53° to 71° with increasing chitosan amount,[41] and for chitosan-hydroxyapatite coatings on nanotitania layer, all samples were hydrophilic, possessing a contact angle of 20–25°.[42]

A comparison of adhesion reported by different authors is extremely difficult as three different methods have been used: a qualitative tape test, a quantitative pull-out test with stress measured, and a nanoscratch test with force measured. As concerns the tape test results, positive opinions have been given for the coating composed of calcium phosphate, titanium oxide, and chitosan oligosaccharide lactate,[43] titanium diboride – chitosan,[44] the coating comprising of carbon nanotubes, hydroxyapatite, biocompatible macromolecules of kappa-Carrageenan, and chitosan,[45] the catechol functionalized chitosan and gelatin with Ag nanoparticles,[39] and composite coating of hydroxyapatite, bioglass, iron oxide particles and chitosan.[46] For the pull-out method, the bonding between the hydrogels of different chitosan concentrations and titanium alloy substrates ranged from 1.94 MPa to 3.36 MPa.[38] In nanoscratch tests, the reported values were 434 mN for chitosan/gelatin hydrogel,[47] 7.19 mN for HAp/Ti, and 10.4 mN for HAp/MgO interface, with no determined bond strength between a substrate and a coating,[48] and between 16.2 and 33.2 mN for chitosan-ZnO.[49] The last values are similar to those obtained in our research, 4.92 mN and 5.10 mN, for acidic and CO_2 preparation ways, respectively. The employed titanium alloy substrate possessed low roughness, which could also result in poor adhesion of coatings to the substrate. A roughened surface should promote the improvement of coatings' adhesion to the substrate, as the coating-substrate interface increases.

Corrosion resistance was reported several times in recent literature. The ratio of the corrosion rate of coated sample to that of bare titanium was 12–18% for alginate – chitosan coating,[50] 16% for the catechol functionalized chitosan and gelatin implemented with Ag nanoparticles,[39] for Ag-doped TCP-chitosan composite coating of 26–85% of corrosion rate of titanium, the best for 5% Ag addition,[46] for HAp-bioglass and Fe_3O_4 particles between 3% and 23%,[51] and for silver nanoparticles doped chitosan and sodium alginate composite coating the corrosion rate equaled 12–18% of the basic value.[50] However, in[47] for three-dimensional hydrogel nanoclay coating composed of chitosan, gelatin, and halloysite, the corrosion current density was changed between 7.8 nA/cm^2 and 374 nA/cm^2, widely indeed,

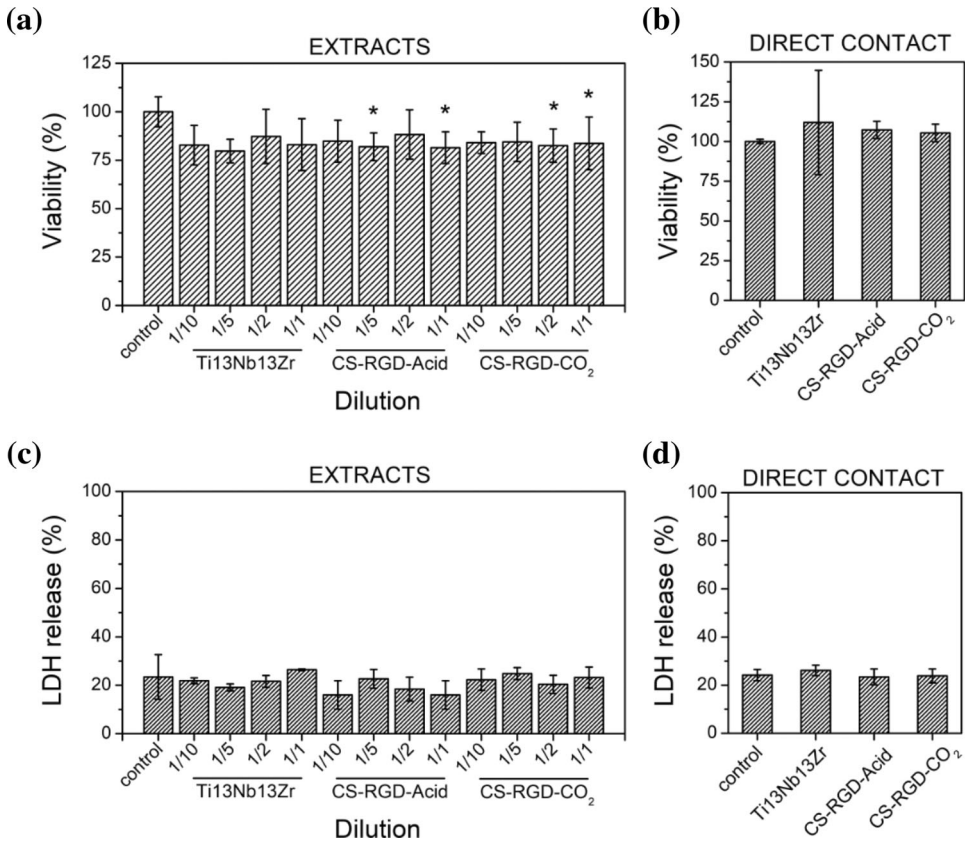

FIGURE 5 The effect of tested materials on viability – for indirect contact (A) and direct contact (B); lactate dehydrogenase release – for indirect contact (C), and direct contact (D); *significantly different from the control (ANOVA with Bonferroni correction $p < .05$).

depending on composition. In our research, the corrosion resistance was almost twice as high after CS-RGD-Acid treatment and over 50% lower for CS-RGD-CO_2 as compared to titanium corrosion in SBF, again similar to a few studies. It seems mentioned that the coatings have not been designed as anticorrosive and the corrosion current density always has remained in a safe area.

Antibacterial efficiency of the proposed here coatings is among the best so far noticed as our results changed between 99% and, in the case of CS-RGD-Acid and *S. aureus* strain, about 99.9999%, i.e. total killing capacity. To compare, in a highly interesting study on this feature, composite coating of chitosan-PVA-silver the antibacterial activity was assessed at and near the surface. Chitosan demonstrated a no-inhibition zone associated with the growth of *E. coli* and *S. aureus*. The antibacterial activity of investigated nanocomposites was enhanced by silver nanoparticles, and at their extremely high content, the bacterial adhesion and growth were stopped.[52] Considering the other results, the antibacterial rate of the composite coating of the catechol functionalized chitosan and gelatin with Ag nanoparticles reached 96–99% against *E. coli* and *S. aureus*,[39] for HAp/MgO coating over 96% against *E. coli* and *S. aureus*,[48] for coating with silver nanoparticles doped chitosan and sodium alginate, the antimicrobial efficiency remained after immersion for 30 days at a level of 96.8%, still a good value.[50] On the other side, in[38] for chitosan-gelatine hydrogel implemented with nanoAg antimicrobial effect against *E. coli* and *S. aureus* reached for 24 h only 70% and 67%, and ~89% reduction in *S. epidermidis* adhesion.[53] A 1.2-fold increase in the antibacterial activity of chitosan/ZnO coating against *E. coli* was detected as compared to the chitosan coating alone.[49] Qualitatively, an antibacterial effect was also reported in vivo 5-day test for the coating of hydroxypropyltrimethyl ammonium chloride chitosan, and in vitro as not only the inhibitive effect on the bacterial adhesion and growth but also prevention of bone destruction was found.[54]

Finally, in our research, considering cytotoxicity, the cell viability based on extracts was over 75%, and for direct contact practically was unchanged. In comparison, in[38] for chitosan-gelatine hydrogel and in another study[40] on silica-chitosan coatings, the osteoblastic cells cultured on the hybrid coating were more viable than those on a pure chitosan coating, and the bare titanium substrate. For the coatings of chitosan combined with Ca^{2+} and Mg^{2+} ions (HAp and MgO), osteoblasts and vascular endothelial cells showed good adhesion and proliferation on the nanocomposite coating.[48] For ALP-PDA coating the number of attached osteoblasts shows an increasing trend over the 7 days except for the last day for which some chemical compositions of coatings showed a lower amount of attached cells than on Ti.[53] Also, the Ag-TCP-chitosan composite coatings did not show any detectable toxicity except for the highest content of silver.[46] It is interesting that when investigating the alginate/chitosan composite coatings, the indirect in vitro cytotoxicity test on the extracts of composite coatings revealed no significant effects on cell viability, but alginate coating more promoted the cells' growth than chitosan coating.[55] Almost no cytotoxicity was observed for multi-walled carbon nanotubes joined to KCG@MHAp.[45] A gallium-modified chitosan/poly

(acrylic acid) bilayer influenced positively MG-63 adhesion and proliferation, but the results were significantly dependent on the day of examination.[56] For a biocomposite coating comprising chitosan and ZnO deposited on a porous Ti, a good cytocompatibility in MG-63 cells was observed as compared to pure Ti; the cell attachment values of Ti and a coating were 92.8% and 91.4%, and the last specimens demonstrated the cell variability over 98% of the control group.[49] A three-dimensional hydrogel nanoclay coating also induced osteoblast viability.[47] The composite coating of hydroxyapatite, bioglass, and iron oxide particles displayed significant cell proliferation relative to the Ti13Nb13Zr alloy.[51] The silicon-chitosan coating demonstrated also that the hybrid coatings were not cytotoxic and promoted cell proliferation on their surfaces,[41] and the chitosan-ZnO coating also showed no cytotoxic responses in MG-63 cells.[49]

4 | CONCLUSIONS

Chitosan coatings with attached RGD peptide on a Ti13Nb13Zr alloy substrate were successfully deposited by electrophoresis using various suspension preparation methods. The RGD peptide did not detach from the chitosan chain during coating deposition.

The adoption of different methods of preparing suspensions for deposition, i.e., dissolution in hydroxyacetic acid or CO_2 saturation, resulted in significant differences in the wettability and thickness of coatings with almost the same roughness of these surfaces. The second method produced a sample with higher corrosion resistance, but both types of coatings adhered relatively weakly to the substrates.

Both coatings demonstrated highly efficient antimicrobial activity, especially for Gram-positive bacteria. The tests on the human hFOB 1.19 osteoblasts cell line showed also sufficient biocompatibility expressed by the viability of cells on the surfaces of proposed coatings.

The novel solution can be assumed as among the best as regards antibacterial activity, with sufficiently low cytotoxicity, expected hydrophilicity, and good corrosion resistance. Both applied procedures give similar results and can be taken into account in further research aimed to improve the adhesion to the substrate and studies in vivo.

ACKNOWLEDGMENTS

Special gratitude to Ms. Aleksandra Laska from the Institute of Manufacturing and Materials Technology, Faculty of Mechanical Engineering and Ship Technology, Gdańsk University of Technology, for her assistance in conducting the AFM examination and scratch test. This research received no external funding.

CONFLICT OF INTEREST STATEMENT

There are no conflicts of interest to declare.

DATA AVAILABILITY STATEMENT

The data that support the findings of this study are available from the corresponding author upon reasonable request.

ORCID

Łukasz Pawłowski https://orcid.org/0000-0002-3321-9207
Szymon Mania https://orcid.org/0000-0003-2748-0393
Adrianna Banach-Kopeć https://orcid.org/0000-0003-2992-7611
Michał Bartmański https://orcid.org/0000-0003-0185-6460
Anna Ronowska https://orcid.org/0000-0001-5715-1211
Kacper Jurak https://orcid.org/0000-0001-9573-8785
Aleksandra Mielewczyk-Gryń https://orcid.org/0000-0001-6795-3840
Natalia Karska https://orcid.org/0000-0003-2429-4157
Sylwia Rodziewicz-Motowidło https://orcid.org/0000-0002-4471-5951
Andrzej Zieliński https://orcid.org/0000-0002-5395-9309

REFERENCES

1. Alipal J, Mohd Pu'ad NAS, Nayan NHM, et al. An updated review on surface functionalisation of titanium and its alloys for implants applications. *Mater Today Proc*. 2021;42:270-282. doi:10.1016/j.matpr.2021.01.499
2. Lin L, Wang H, Ni M, et al. Enhanced osteointegration of medical titanium implant with surface modifications in micro/nanoscale structures. *J Orthop Transl*. 2014;2:35-42. doi:10.1016/J.JOT.2013.08.001
3. Bansal P, Singh G, Sidhu HS. Improvement of surface properties and corrosion resistance of Ti13Nb13Zr titanium alloy by plasma-sprayed HA/ZnO coatings for biomedical applications. *Mater Chem Phys*. 2021;257:123738. doi:10.1016/J.MATCHEMPHYS.2020.123738
4. Tao B, Zhao W, Lin C, et al. Surface modification of titanium implants by ZIF-8@Levo/LBL coating for inhibition of bacterial-associated infection and enhancement of in vivo osseointegration. *Chem Eng J*. 2020;390:124621. doi:10.1016/J.CEJ.2020.124621
5. Souza JCM, Sordi MB, Kanazawa M, et al. Nano-scale modification of titanium implant surfaces to enhance osseointegration. *Acta Biomater*. 2019;94:112-131. doi:10.1016/j.actbio.2019.05.045
6. Stróż A, Łosiewicz B, Zubko M, et al. Production, structure and biocompatible properties of oxide nanotubes on Ti13Nb13Zr alloy for medical applications. *Mater Charact*. 2017;132:363-372. doi:10.1016/J.MATCHAR.2017.09.004
7. Sunil BR, Kranthi Kiran AS, Ramakrishna S. Surface functionalized titanium with enhanced bioactivity and antimicrobial properties through surface engineering strategies for bone implant applications. *Curr Opin Biomed Eng*. 2022;23:100398. doi:10.1016/J.COBME.2022.100398
8. Pawłowski Ł, Bartmański M, Mielewczyk-Gryń A, Zieliński A. Effects of surface pretreatment of titanium substrates on properties of Electrophoretically deposited biopolymer chitosan/Eudragit E 100 coatings. *Coatings*. 2021;11:1120. doi:10.3390/coatings11091120
9. Besra L, Liu M. A review on fundamentals and applications of electrophoretic deposition (EPD). *Prog Mater Sci*. 2007;52:1-61. doi:10.1016/j.pmatsci.2006.07.001
10. Simchi A, Pishbin F, Boccaccini AR. Electrophoretic deposition of chitosan. *Mater Lett*. 2009;63:2253-2256. doi:10.1016/j.matlet.2009.07.046
11. Sorkhi L, Farrokhi-Rad M, Shahrabi T. Electrophoretic deposition of chitosan in different alcohols. *J Coatings Technol Res*. 2014;11:739-746. doi:10.1007/s11998-014-9578-7
12. Jiang T, Zhang Z, Zhou Y, et al. Surface functionalization of titanium with chitosan/gelatin via electrophoretic deposition: characterization and cell behavior. *Biomacromolecules*. 2010;11:1254-1260. doi:10.1021/bm100050d
13. Pawłowski Ł, Bartmański M, Mielewczyk-Gryń A, Cieślik BM, Gajowiec G, Zieliński A. Electrophoretically deposited chitosan/Eudragit E 100/AgNPs composite coatings on titanium substrate as a

silver release system. *Materials (Basel)*. 2021;14:4533. doi:10.3390/ma14164533
14. Du Y-Z, Cai PL, Li X, et al. RGD peptide-mediated chitosan-based polymeric micelles targeting delivery for integrin-overexpressing tumor cells. *Int J Nanomedicine*. 2011;6:3499-3508. doi:10.2147/IJN.S26670
15. Bellis SL. Advantages of RGD peptides for directing cell association with biomaterials. *Biomaterials*. 2011;32:4205-4210. doi:10.1016/j.biomaterials.2011.02.029
16. Chen WY, Chen YT, Ke CJ, Chen CY, Lin FH. The synthesis and evaluation of RGD−conjugated chitosan gel as daily supplement for body weight control. *Materials (Basel)*. 2021;14:4467. doi:10.3390/ma14164467
17. Hennessy KM, Clem WC, Phipps MC, Sawyer AA, Shaikh FM, Bellis SL. The effect of RGD peptides on osseointegration of hydroxyapatite biomaterials. *Biomaterials*. 2008;29:3075-3083. doi:10.1016/j.biomaterials.2008.04.014
18. Nayak S, Dey T, Naskar D, Kundu SC. The promotion of osseointegration of titanium surfaces by coating with silk protein sericin. *Biomaterials*. 2013;34:2855-2864. doi:10.1016/j.biomaterials.2013.01.019
19. Shi Z, Neoh KG, Kang ET, Poh C, Wang W. Bacterial adhesion and osteoblast function on titanium with surface-grafted chitosan and immobilized RGD peptide. *J Biomed Mater Res Part A*. 2008;86A:865-872. doi:10.1002/JBM.A.31648
20. Yadav AS, Radharani NNV, Gorain M, et al. RGD functionalized chitosan nanoparticle mediated targeted delivery of raloxifene selectively suppresses angiogenesis and tumor growth in breast cancer. *Nanoscale*. 2020;12:10664-10684. doi:10.1039/C9NR10673A
21. Tsai WB, Chen YR, Liu HL. RGD-conjugated crosslinked chitosan scaffolds for culture and osteogenic differentiation of mesenchymal stem cells. *J Taiwan Inst Chem Eng*. 2013;44:1-7. doi:10.1016/J.JTICE.2012.09.003
22. Chua PH, Neoh KG, Kang ET, Wang W. Surface functionalization of titanium with hyaluronic acid/chitosan polyelectrolyte multilayers and RGD for promoting osteoblast functions and inhibiting bacterial adhesion. *Biomaterials*. 2008;29:1412-1421. doi:10.1016/J.BIOMATERIALS.2007.12.019
23. Gorczyca G, Tylingo R, Szweda P, Augustin E, Sadowska M, Milewski S. Preparation and characterization of genipin cross-linked porous chitosan–collagen–gelatin scaffolds using chitosan–CO2 solution. *Carbohydr Polym*. 2014;102:901-911. doi:10.1016/J.CARBPOL.2013.10.060
24. Khokhlova MA, Gallyamov MO, Khokhlov AR. Chitosan nanostructures deposited from solutions in carbonic acid on a model substrate as resolved by AFM. *Colloid Polym Sci*. 2012;290:1471-1480. doi:10.1007/s00396-012-2673-3
25. Sakai Y, Hayano K, Yoshioka H, Yoshioka H. A novel method of dissolving chitosan in water for industrial application. *Polym J*. 2001;33:640-642. doi:10.1295/polymj.33.640
26. Tylingo R, Kempa P, Banach-Kopeć A, Mania S. A novel method of creating thermoplastic chitosan blends to produce cell scaffolds by FDM additive manufacturing. *Carbohydr Polym*. 2022;280:119028. doi:10.1016/J.CARBPOL.2021.119028
27. Pawłowski Ł, Bartmański M, Strugała G, Mielewczyk-Gryń A, Jażdżewska M, Zieliński A. Electrophoretic deposition and characterization of chitosan/Eudragit E 100 coatings on titanium substrate. *Coatings*. 2020;10:607. doi:10.3390/coatings10070607
28. Pawłowski Ł, Bartmański M, Mielewczyk-Gryń A, Zieliński A. Chitosan/-poly(4-vinylpyridine) coatings formed on AgNPs-decorated titanium. *Mater Lett*. 2022;319:132293. doi:10.1016/j.matlet.2022.132293
29. Loch J, Krawiec H. Corrosion behaviour of cobalt alloys in artificial saliva solution. *Arch Foundry Eng*. 2013;13:101-106.
30. Pawłowski Ł, Wawrzyniak J, Banach-Kopeć A, et al. Antibacterial properties of laser-encapsulated titanium oxide nanotubes decorated with nanosilver and covered with chitosan/Eudragit polymers. *Biomater Adv*. 2022;138:212950. doi:10.1016/j.bioadv.2022.212950
31. Farrokhi-Rad M, Fateh A, Shahrabi T. Effect of pH on the electrophoretic deposition of chitosan in different alcoholic solutions. *Surfaces and Interfaces*. 2018;12:145-150. doi:10.1016/J.SURFIN.2018.05.010
32. Corni I, Ryan MP, Boccaccini AR. Electrophoretic deposition: from traditional ceramics to nanotechnology. *J Eur Ceram Soc*. 2008;28:1353-1367. doi:10.1016/j.jeurceramsoc.2007.12.011
33. Queiroz MF, Melo KRT, Sabry DA, Sassaki GL, Rocha HAO. Does the use of chitosan contribute to oxalate kidney stone formation? *Mar Drugs*. 2015;13:141-158. 13 (2014) 141–158. doi:10.3390/MD13010141
34. Brun P, Zamuner A, Battocchio C, et al. Bio-functionalized chitosan for bone tissue engineering. *Int J Mol Sci*. 2021;22:1-18. doi:10.3390/ijms22115916
35. Renoud P, Toury B, Benayoun S, Attik G, Grosgogeat B. Functionalization of titanium with chitosan via silanation: evaluation of biological and mechanical performances. *PLoS One*. 2012;7:e39367. doi:10.1371/journal.pone.0039367
36. Kouchak M, Handali S, Naseri Boroujeni B. Evaluation of the mechanical properties and drug permeability of chitosan/Eudragit RL composite film, Osong public heal. *Res Pers*. 2015;6:14-19. doi:10.1016/j.phrp.2014.12.001
37. Lund PA, De Biase D, Liran O, et al. Understanding how microorganisms respond to acid pH is central to their control and successful exploitation. *Front Microbiol*. 2020;11:556140. doi:10.3389/fmicb.2020.556140
38. Wu X, Liu S, Chen K, et al. 3D printed chitosan-gelatine hydrogel coating on titanium alloy surface as biological fixation interface of artificial joint prosthesis. *Int J Biol Macromol*. 2021;182:669-679. doi:10.1016/j.ijbiomac.2021.04.046
39. Ren L, Zhao Y, Yang L, et al. Preparation and characterization of the catechol functionalized chitosan-Ag NPs deposited onto titanium surface. *Surf Coatings Technol*. 2021;420:127319. doi:10.1016/J.SURFCOAT.2021.127319
40. Jun SH, Lee EJ, Yook SW, Kim HE, Kim HW, Koh YH. A bioactive coating of a silica xerogel/chitosan hybrid on titanium by a room temperature sol-gel process. *Acta Biomater*. 2010;6:302-307. doi:10.1016/j.actbio.2009.06.024
41. Palla-Rubio B, Araújo-Gomes N, Fernández-Gutiérrez M, et al. Synthesis and characterization of silica-chitosan hybrid materials as antibacterial coatings for titanium implants. *Carbohydr Polym*. 2019;203:331-341. doi:10.1016/j.carbpol.2018.09.064
42. Pawlik A, Rehman MAU, Nawaz Q, Bastan FE, Sulka GD, Boccaccini AR. Fabrication and characterization of electrophoretically deposited chitosan-hydroxyapatite composite coatings on anodic titanium dioxide layers. *Electrochim Acta*. 2019;307:465-473. doi:10.1016/j.electacta.2019.03.195
43. Pantović Pavlović MR, Pavlović MM, Eraković S, Stevanović JS, Panić VV, Ignjatović N. Simultaneous anodization/anaphoretic electrodeposition synthesis of nano calcium phosphate/titanium oxide composite coatings assisted with chitosan oligosaccharide lactate. *Mater Lett*. 2020;261:1-4. doi:10.1016/j.matlet.2019.127121
44. Varlık Ö, Göncü Y, Ay N. Electrophoretic deposition of composite titanium diboride-chitosan coating. *Mater Chem Phys*. 2022;282:125927. doi:10.1016/j.matchemphys.2022.125927
45. Chen M, Zhang H, Shan S, Li Y, Li X, Peng D. Fabrication of multi-walled carbon nanotubes/carrageenan-chitosan@ Ce and Sr substituted hydroxyapatite biocomposite coating on titanium: In vivo bone formation evaluations. *J King Saud Univ - Sci*. 2020;32:1175-1181. doi:10.1016/j.jksus.2019.11.006
46. Singh RK, Awasthi S, Dhayalan A, Ferreira JMF, Kannan S. Deposition, structure, physical and invitro characteristics of Ag-doped β-Ca3(PO4)2/chitosan hybrid composite coatings on titanium metal. *Mater Sci Eng C*. 2016;62:692-701. doi:10.1016/j.msec.2016.02.013
47. Alipal J, Saidin S, Abdullah HZ, Idris MI, Lee TC. Physicochemical and cytotoxicity studies of a novel hydrogel nanoclay EPD coating on

titanium made of chitosan/gelatin/halloysite for biomedical applications. *Mater Chem Phys*. 2022;290:126543. doi:10.1016/j.matchemphys.2022.126543

48. Zhang X, Yin H, Xiao L, et al. Chitosan regulated electrochemistry for dense hydroxyapatite/MgO nanocomposite coating with antibiosis and osteogenesis on titanium alloy. *Colloids Interface Sci Commun*. 2022;48:100616. doi:10.1016/j.colcom.2022.100616
49. Lin MH, Wang YH, Kuo CH, et al. Hybrid ZnO/chitosan antimicrobial coatings with enhanced mechanical and bioactive properties for titanium implants. *Carbohydr Polym*. 2021;257:117639. doi:10.1016/j.carbpol.2021.117639
50. Duan Y, Wu Y, Yan R, Lin M, Sun S, Ma H. Chitosan-sodium alginate-based coatings for self-strengthening anticorrosion and antibacterial protection of titanium substrate in artificial saliva. *Int J Biol Macromol*. 2021;184:109-117. doi:10.1016/J.IJBIOMAC.2021.06.042
51. Singh S, Singh G, Bala N. Characterization, electrochemical behavior and in vitro hemocompatibility of hydroxyapatite-bioglass-iron oxide-chitosan composite coating by electrophoretic deposition. *Surf Coatings Technol*. 2021;405:126564. doi:10.1016/j.surfcoat.2020.126564
52. Mishra SK, Ferreira JMF, Kannan S. Mechanically stable antimicrobial chitosan-PVA-silver nanocomposite coatings deposited on titanium implants. *Carbohydr Polym*. 2015;121:37-48. doi:10.1016/j.carbpol.2014.12.027
53. Zheng D, Neoh KG, Kang ET. Bifunctional coating based on carboxymethyl chitosan with stable conjugated alkaline phosphatase for inhibiting bacterial adhesion and promoting osteogenic differentiation on titanium. *Appl Surf Sci*. 2016;360:86-97. doi:10.1016/j.apsusc.2015.11.003
54. Kodama J, Chen H, Zhou T, et al. Antibacterial efficacy of quaternized chitosan coating on 3D printed titanium cage in rat intervertebral disc space. *Spine J*. 2021;21:1217-1228. doi:10.1016/j.spinee.2021.02.016
55. Wang Y, Guo X, Pan R, et al. Electrodeposition of chitosan/gelatin/-nanosilver: a new method for constructing biopolymer/nanoparticle composite films with conductivity and antibacterial activity. *Mater Sci Eng C*. 2015;53:222-228. doi:10.1016/j.msec.2015.04.031
56. Bonifacio MA, Cometa S, Dicarlo M, et al. Gallium-modified chitosan/poly(acrylic acid) bilayer coatings for improved titanium implant performances. *Carbohydr Polym*. 2017;166:348-357. doi:10.1016/j.carbpol.2017.03.009

How to cite this article: Pawłowski Ł, Mania S, Banach-Kopeć A, et al. Osteoblast and bacterial cell response on RGD peptide-functionalized chitosan coatings electrophoretically deposited from different suspensions on Ti13Nb13Zr alloy. *J Biomed Mater Res*. 2023;1-13. doi:10.1002/jbm.b.35286